energies

Article

Wireless Battery Chargers Operating at Multiple Switching Frequencies with Improved Performance

Deniss Stepins [1,*], Aleksandrs Sokolovs [1], Janis Zakis [1] and Ouseph Charles [2]

1 Institute of Industrial Electronics and Electrical Engineering, Riga Technical University, LV-1048 Riga, Latvia; aleksandrs.sokolovs@rtu.lv (A.S.); janis.zakis@rtu.lv (J.Z.)
2 Dyninno Ltd., LV-1010 Riga, Latvia
* Correspondence: deniss.stepins@rtu.lv

Abstract: The operation of wireless battery chargers at multiple switching frequencies may lead to a noticeable suppression of conducted and radiated electromagnetic interference (EMI) at the cost of decreased efficiency (mainly at lower load resistances) and increased peak and root mean square values of currents of power components of the wireless battery charger. Moreover, the reduction in conducted EMI is only moderate (<8.3 dB). Therefore, a novel approach based on modified resonant circuits and a modified control technique to obtain better reduction in the conducted and radiated EMI without significantly compromising other performance characteristics of the wireless battery charger is proposed and validated by using simulations and experiments. It is shown in this paper that the wireless charger operating at multiple switching frequencies with the proposed approach for the performance improvement has a more effective implementation of the four-switching frequency spread-spectrum technique with better conducted and radiated EMI reduction at all load resistances, lower values of peak and RMS currents at all load resistances, and higher efficiency in constant current mode and in the beginning of constant voltage mode (at lower values of the load resistances) than that of the conventional wireless charger operating at multiple switching frequencies.

Keywords: wireless battery charger; inductive-resonant; spread spectrum; electromagnetic interference; efficiency

check for updates

Citation: Stepins, D.; Sokolovs, A.; Zakis, J.; Charles, O. Wireless Battery Chargers Operating at Multiple Switching Frequencies with Improved Performance. *Energies* **2023**, *16*, 3734. https://doi.org/10.3390/en16093734

Academic Editor: Sheldon Williamson

Received: 10 April 2023
Revised: 25 April 2023
Accepted: 26 April 2023
Published: 27 April 2023

1. Introduction

With the rapid development of mobile electrical and electronic technologies, electric power transfer without wires has become one of the most topical research directions in the field of electrical and power engineering nowadays, because the approach of transferring electric power has a variety of advantages including better reliability, better convenience, and so on. Due to these advantages, wireless power transfer (WPT) has gained substantial popularity, especially for the static or dynamic charging of electrical autonomous mobile robots (AMR) or electrical automated guided vehicles (AGV) [1–4]. There are two main approaches for charging AMR or AGV: (1) the transmitting coil is buried in the floor, but the receiving coil is placed at the bottom of the AMR or AGV and (2) the transmitting coil is attached to the wall, but the receiving coil is attached to the side of the AGV or AMR (see Figure 1).

When designing a wireless battery charger, electromagnetic compatibility (EMC) issues should also be considered, because they are significant sources of conducted and radiated electromagnetic interference (EMI) to sensitive electronic devices [5–10], as is depicted in Figure 1a. Therefore, different national or international EMC standards specify the limits and measurement methods of EMI of the wireless battery chargers. Since WPT systems are often regarded as industrial devices, they should comply with the international standard CISPR11 requirements.

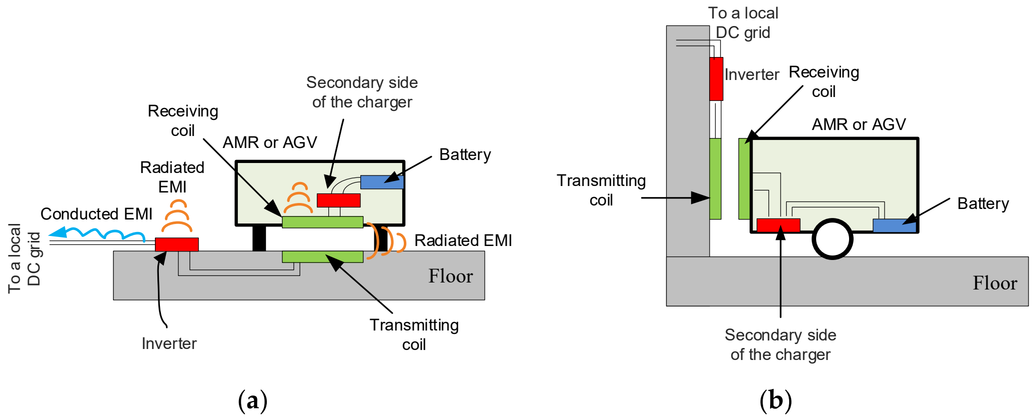

Figure 1. Wireless charging of AGV or AMR. (**a**) the transmitting coil is buried in the floor, and (**b**) the transmitting coil is attached to the wall.

Different approaches for the reduction in the conducted and radiated EMI generated by switching power converters (and, of course, inductive-resonant WPT systems) have been proposed. Classical approaches to reduce the conducted EMI are EMI filters, but for the suppression of the radiated EMI, shielding is used. Although less effective (in terms of EMI suppression), the spread-spectrum approach has gained substantial popularity over the last two decades because it can be used for suppressing conducted and radiated EMI simultaneously and can be implemented by using a suitable program code for a microcontroller. The spread-spectrum technique was initially used for the suppression of EMI from traditional switching power converters [11,12], and recently, it was applied to inductive-resonant WPT systems (including wireless battery chargers) [5,7–9]. Several types of the spread-spectrum technique exist for EMI reduction from wireless battery chargers, but the multi-switching frequency technique is preferable to other spread-spectrum techniques for wireless battery chargers because it can be implemented by using a relatively inexpensive microcontroller that can be used simultaneously for implementing constant current (CC) or constant voltage (CV) battery charging modes [9]. One of the drawbacks of the multi-switching frequency technique (as well as the other spread-spectrum techniques) is that the peak value of coil currents may increase significantly [9]. Another drawback of the technique is that EMI reduction is only moderate (up to 8.3 dB for the conducted EMI (if the standard 9 kHz resolution bandwidth of a spectrum analyzer is used) [9] and up to 4 dB for the radiated EMI (if the close-to-standard 10 kHz resolution bandwidth of a spectrum analyzer is used) [5]). Higher EMI reduction can still be achieved with the multi-switching frequency technique, if a higher number of frequencies are used, but this would inevitably lead to a larger difference between the minimum and maximum switching frequencies Δf and it would result in a higher drop in the efficiency in CC mode (at lower value of the equivalent input resistance of a battery) and a more significant increase in the peak and RMS values of currents of power components of the wireless battery charger [9]. Therefore, a novelty of this paper is an approach to improve the reduction in conducted and radiated EMI without significantly compromising other performance characteristics of the wireless battery charger. It will be shown in this paper that the approach based on a modification of the resonant tank and correct selection of parameters of the multi-switching frequency technique will lead to a more effective implementation of the four-switching frequency spread-spectrum technique, giving better conducted and radiated EMI reduction at all load resistances, lower values of peak and RMS currents at all load resistances, and higher efficiency in constant current mode and in the beginning of constant voltage mode (at lower values of the load resistances) than that of the conventional wireless charger operating at multiple switching frequencies.

This article is partly based on a paper [13] originally presented in the Proceedings of 2021 IEEE 19th International Power Electronics and Motion Control conference (PEMC).

This paper is organized as follows: a simulation-based analysis of a conventional wireless charger operating at either a single or multiple frequencies and a wireless charger operating at multiple frequencies with the proposed approach for the performance improvement is presented in detail in Section 2; the experimental setup, results, and discussion are presented in Section 3; and finally, conclusions are given in Section 4.

2. Simulation-Based Analysis of the Wireless Charger Performance

2.1. Analysis of the Conventional Wireless Charger Operating at a Single Frequency or Multiple Frequencies

PSIM software will be used in the simulation-based analysis of the performance of the wireless battery charger. A block diagram of the conventional wireless battery charger operating at a single switching frequency (without a spread spectrum) or at multiple switching frequencies (with a spread spectrum) is shown in Figure 2. The microcontroller (MCU1) with a receiver receives the output voltage and current digital values from the transmitter of the microcontroller (MCU2). Based on these values, MCU1 computes the duty cycles to control the metal–oxide–semiconductor field-effect transistors (MOSFETs) of the H-bridge inverter. Thanks to the feedback loop, the CC or CV modes of the charger can be achieved. If the charger operates at multiple frequencies (e.g., at four frequencies), then MCU1 generates control pulses with different frequencies to implement the multi-switching frequency technique to spread EMI noise over a wider frequency range and, thus, to reduce the levels of conducted EMI (Figure 3). The primary and secondary resonant tanks of the conventional wireless charger either operating at a single or multiple frequencies are tuned to the same frequency.

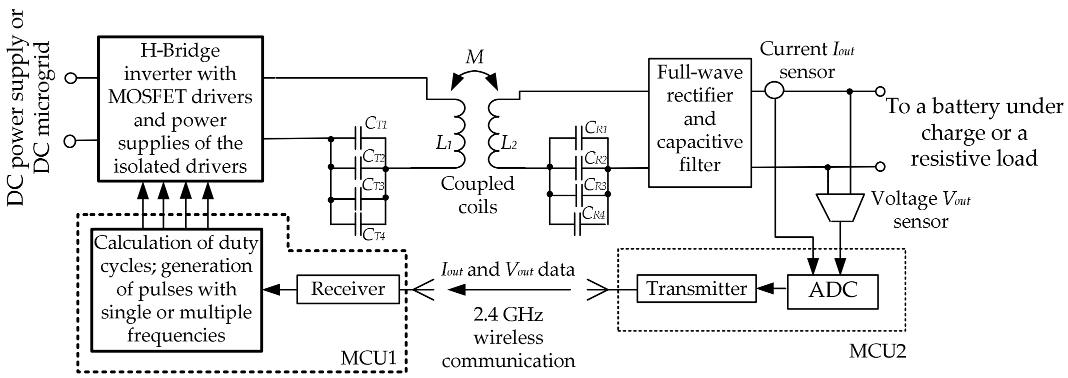

Figure 2. A block diagram of the conventional wireless battery charger operating either at a single switching frequency or at multiple switching frequencies. Note: adapted from [9].

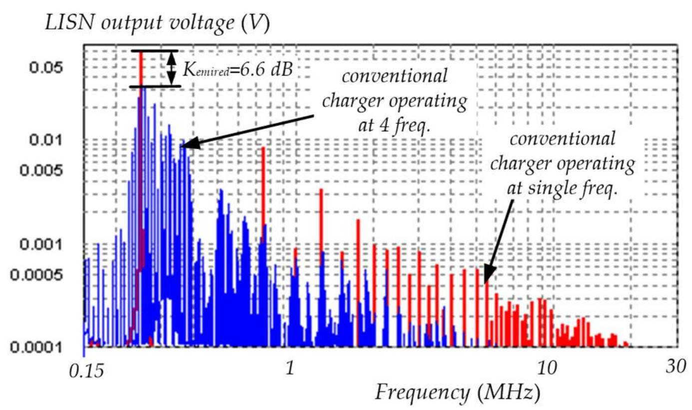

Figure 3. Simulated conducted EMI (LISN output voltage) of the conventional wireless charger operating at a single or four switching frequencies. (V_{in} = 25 V; R_{load} = 12.6 Ω; modulation frequency $f_{\text{m}} \approx 8$ kHz).

To make a comparison of the performance of the proposed wireless charger operating at multiple frequencies with the performance of the conventional wireless charger operating at either a single or multiple switching frequencies, a simulation model of the conventional charger and the proposed charger with the modified resonant tank were created in PSIM. The simulation model of the conventional wireless charger is based on the block diagram presented in Figure 2. The model takes into account typical values of the parasitic resistances of the capacitors, coils, MOSFETs, and the diodes. However, the model does not take into account the switching losses and the fact that the parasitic resistances are frequency-dependent. It is assumed in the model that the input capacitor is a ceramic one with capacitance 10 µF and equivalent series resistance 0.01 Ω. The Bluetooth low-energy wireless communication is not modeled. The losses of the control circuits are not taken into account in the model.

The model of the wireless charger was created according to the specifications presented in Table 1. It is assumed in the model that the resonant tank of the conventional single-frequency wireless charger is tuned to the switching frequency f_1 = 126.48 kHz, but the resonant tank of the conventional multi-frequency wireless charger is tuned to f_2 = 138.87 kHz.

Table 1. Parameters of the conventional wireless battery chargers operating at a single frequency and at multiple frequencies.

Parameter	Conv. Charger Operating at one Frequency	Conv. Charger Operating at Multiple Frequencies
Rated output current in CC mode	2 A	2 A
Rated output voltage in CV mode	25.2 V	25.2 V
Cut-off discharge voltage	22.2 V	22.2 V
DC input voltage	25–30 V	25–30 V
Switching frequencies [1]	126.48 kHz	f_1 = 126.48 kHz f_2 = 138.87 kHz f_3 = 159.97 kHz f_4 = 187.54 kHz
Capacitances of the capacitors of the resonant tanks [2]	$C_{T1} = C_{R1}$ = 4.7 nF $C_{T2} = C_{R2}$ = 22 nF $C_{T3} = C_{R3}$ = 22 nF $C_{T4} = C_{R4}$ = 10 nF	$C_{T1} = C_{R1}$ = 4.7 nF $C_{T2} = C_{R2}$ = 22 nF $C_{T3} = C_{R3}$ = 22 nF
L1 and L2	27 µH	27 µH
Ferrite pad size	10 × 10 cm	10 × 10 cm
Distance between the coils	2.7 cm	2.7 cm
Maximum misalignment of the coils	1 cm	1 cm

[1.] The switching frequencies were calculated for given values of the compensation capacitances by using the Thomson formulas. [2.] The values of the capacitances were selected because they are typical nominal values of polymer film capacitors.

Ansys Maxwell software was used to model and design the coils. The coils were modeled at different misalignments, and it was determined that the mutual inductance between the coils is 8.61 µH in the worst-case lateral misalignment (see Figure 4).

The simulations in PSIM were carried out for the worst-case misalignment, and the main simulation results for different load resistances (battery input equivalent resistances) are presented in Figures 3, 5 and 6 and Table 2. The conducted EMI reduction coefficient (K_{emired}) as the difference between the maximum levels of EMI for two different cases was calculated from the simulation results to estimate the EMI reduction potential. A line impedance stabilization network (LISN) model was connected between the DC voltage source and the charger circuit during the simulations. The LISN model is described in, e.g., [9] or [13].

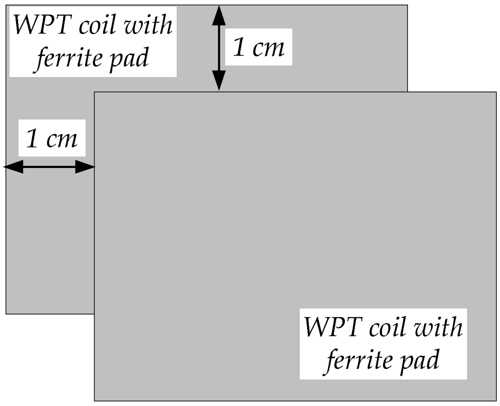

Figure 4. A top view of WPT coils with the worst-case lateral misalignment.

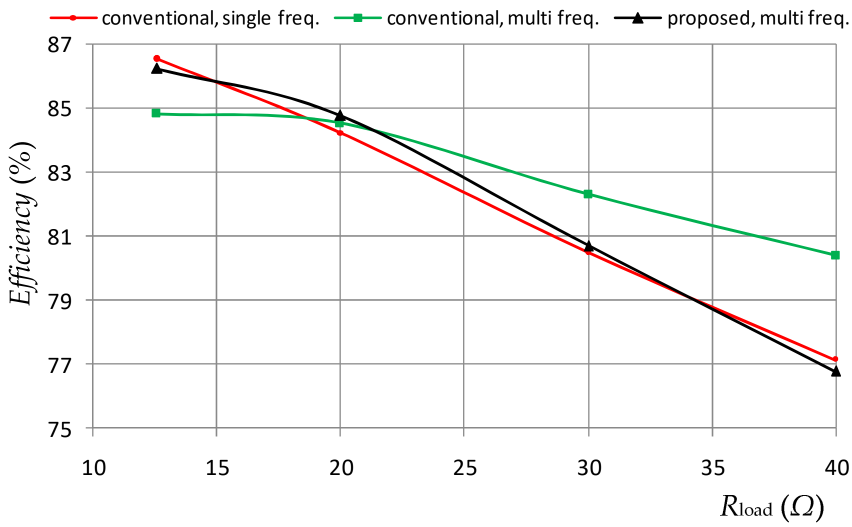

Figure 5. The simulated efficiency versus the load resistance for the three different cases (with the worst coupling): the conventional wireless charger operating at a single frequency (red); the conventional wireless charger operating at four frequencies (green); and the wireless charger operating at four frequencies with the proposed modified resonant tank (black).

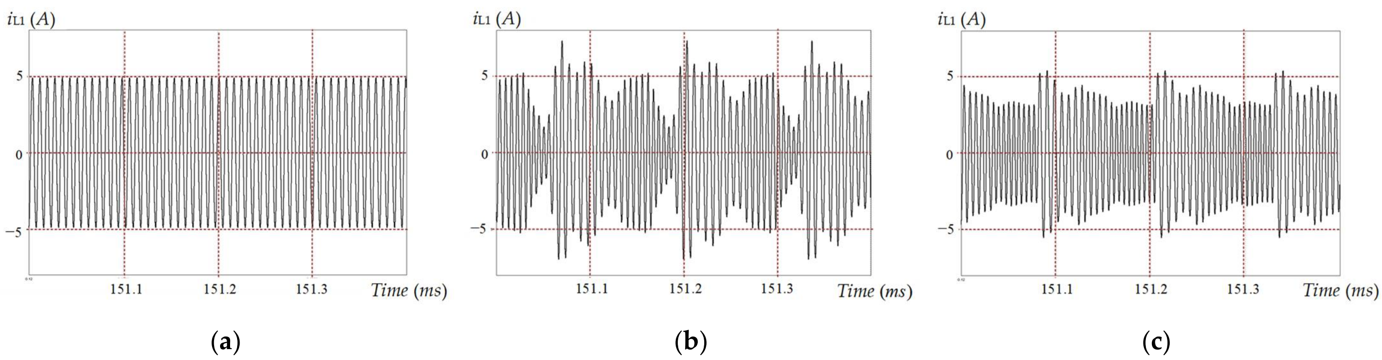

Figure 6. The simulated current waveform of the transmitting coil for three different cases (with the worst coupling): (**a**) the conventional wireless charger operating at a single frequency; (**b**) the conventional wireless charger operating at four frequencies; and (**c**) the wireless charger operating at four frequencies with the proposed modified control technique and resonant tank. Parameters: CC mode; R_{load} = 12.6 Ω; V_{in} = 25 V; $f_m \approx 8$ kHz.

Table 2. The simulation results (with the worst-case coupling).

Parameter	R_{load} (Ω)	Classical Approach (the Charger Operates at a Single Frequency)	Classical Approach (the Charger Operates at four Frequencies w/o Modification of the Res. Tank)	Proposed Approach (the Charger Operates at four Frequencies with Modification of the Res. Tank)
K_{emired} (dB)	12.6	-	6.6	10.31
	20	-	5.34	8.36
	30	-	4.93	7.84
	40	-	3.9	7.67
I_{peakL1} (A)	12.6	4.87	7.3	5.24
	20	4.79	6.41	5.23
	30	4.67	5.86	5.1
	40	4.61	5.29	4.86
I_{RMSL1} (A)	12.6	3.53	3.4	2.9
	20	3.49	3.08	2.87
	30	3.46	2.93	2.84
	40	3.42	2.8	2.81
I_{peakL2} (A)	12.6	3.32	5.27	4.59
	20	2.55	3.67	2.98
	30	1.65	2.95	1.99
	40	1.3	2.71	1.54
I_{RMSL2} (A)	12.6	2.27	2.45	2.24
	20	1.47	1.68	1.47
	30	1.03	1.23	1
	40	0.79	0.98	0.77
I_{RMSQ1} (A)	12.6	2.27	2.24	1.99
	20	1.86	1.78	1.69
	30	1.55	1.47	1.42
	40	1.37	1.27	1.26
I_{RMSQ3} (A)	12.6	2.7	2.49	2.1
	20	2.95	2.51	2.32
	30	3.09	2.53	2.45
	40	3.14	2.55	2.51

Note: I_{peakL1} is the peak value of the current of the coil L1; I_{peakL2} is the peak value of the current of the coil L2; I_{RMSL1} is the RMS value of the current of the coil L1; I_{RMSL2} is the RMS value of current of the coil L2; I_{RMSQ1} is the RMS value of the current of the left high-side MOSFET; I_{RMSQ3} is the RMS value of the current of the right low-side MOSFET. It should also be noted that in the case of the conventional wireless charger operating at multiple frequencies, $N_1 = N_2 = N_3 = N_4 = 5$ and $f_m \approx 8$ kHz, but in the case of the wireless charger operating at multiple frequencies with the proposed approach for the performance improvement, $N_1 = N_2 = 3$, $N_3 = 5$, $N_4 = 9$, and $f_m \approx 8$ kHz.

As well as the coefficient of EMI reduction and the efficiency, we also analyzed peak values of the WPT coils (because they affect the choice of the ferrite pads; higher peak values of the currents of the coils will require ferrite pads with higher saturation fields, which are more expensive), RMS values of the currents of the WPT coils (because they affect the choice of the cross-sectional area of the litz wire), and RMS values of the currents of the MOSFETs (because they affect the heatsink area).

Through the simulation-based comparative analysis of the performance characteristics of the conventional wireless chargers operating at multiple frequencies and that of the wireless chargers operating at a single frequency, we can conclude that:

- The operation of the wireless charger at multiple frequencies leads to significant reduction in the conducted EMI. However, the coefficient of the reduction in EMI decreases as the load resistance increases. However, this may not be a problem in terms of complying with EMC standards, because at a higher R_{load}, EMI levels are lower.
- The peak values of the currents of the transmitting coil of the conventional wireless charger operating at multiple switching frequencies are much higher (up to 50%) at

a lower R_{load} (in CC mode and in the beginning of CV mode), but the percentage difference goes down as R_{load} increases.
- The peak values of the currents of the receiving coil of the conventional wireless charger operating at multiple switching frequencies are much higher (from approximately 50% in CC mode to more than 100% in CV mode at $R_{load} > 40\ \Omega$).
- The RMS values of the currents of the transmitting coil of both types of the conventional wireless chargers have similar values, but at a higher R_{load}, the conventional charger operating at multiple frequencies has moderately lower values.
- The RMS values of the currents of the receiving coil of the conventional wireless charger operating at multiple switching frequencies are moderately higher (the difference increases from 10% to 25% as R_{load} increases).
- The RMS values of the currents of the high-side MOSFETs of the H-bridge inverter are similar for both types of the conventional wireless chargers (at every R_{load}).
- The RMS values of the currents of the low-side MOSFETs of the H-bridge inverter are moderately lower for the conventional wireless charger operating at multiple switching frequencies (especially at a higher R_{load}).
- The conventional wireless charger operating at multiple switching frequencies has noticeably lower efficiency at a lower R_{load} (in CC mode and in the beginning of CV mode) but noticeably higher efficiency in CV mode (when $R_{load} > 30\ \Omega$) than that of the wireless charger operating at a single frequency. The simulations also revealed that the difference between the efficiencies becomes even higher at lower mutual inductances in CC mode. It should be noted that the increase in the efficiency at higher load resistances may not be so noticeable in a real life, because the simulation model does not take into account the switching losses and the fact that the parasitic resistances of the components are frequency-dependent.

2.2. Analysis of the Wireless Charger Operating at Multiple Frequencies with the Proposed Control Approach and Modified Resonant Tank

In order to significantly reduce the peak values of the currents of the WPT coils, increase the efficiency at lower load resistances (mainly in CC mode), and significantly improve the conducted EMI reduction without degrading RMS values of the currents, a modified control approach and resonant circuits are proposed, as shown in Figure 7. The resonant circuits consist of the same capacitors and WPT coils, but capacitors C_{T3}, C_{T4}, C_{R3}, and C_{R4} are connected in series with MOSFETs (Q_{T1}, Q_{T2}, Q_{R1}, and Q_{R2}, respectively). The transistors are used as switches to tune the resonant circuits to the resonance for given switching frequencies. For example, if the wireless charger operates at f_1 = 126.48 kHz, then all the transistors are on; if the wireless charger operates at f_4 = 187.54 kHz, then the transistors are off, and so on. Since the charger has two transistors in each resonant tank, the resonant tanks can be tuned to four different frequencies according to their values shown in Table 1. Note that we choose four switching frequencies because even though a higher number of switching frequencies would lead to better EMI reduction, the number of transistors and their drivers would also increase, inevitably leading to an appreciably increased occupied PCB area and number of components. Considering the trade-off between EMI reduction and the number of additional components, we believe that four switching frequencies in the proposed method is the optimum number.

The control signals of the transistors of the primary resonant circuit must be synchronized with those of the secondary resonant circuit. Therefore, the control signals of the transistors (Q_{R1} and Q_{R2}) of the secondary resonant circuit must be transferred from MCU1 wirelessly with a small delay (<0.5 µs). Due to the fact that the Bluetooth low-energy communication has a relatively large delay (up to several tens of ms or even higher) [14,15], for low-delay communication, it is better to use infrared communication, as is recommended in [16]. Therefore, infrared communication (colored in green in Figure 7) is used to transfer the control signals of Q_{R1} and Q_{R2} from MCU1. For a better understanding of the operating principle of the wireless charger with the proposed control approach and modified resonant circuits, important waveforms were obtained through simulations and are presented in Figure 8.

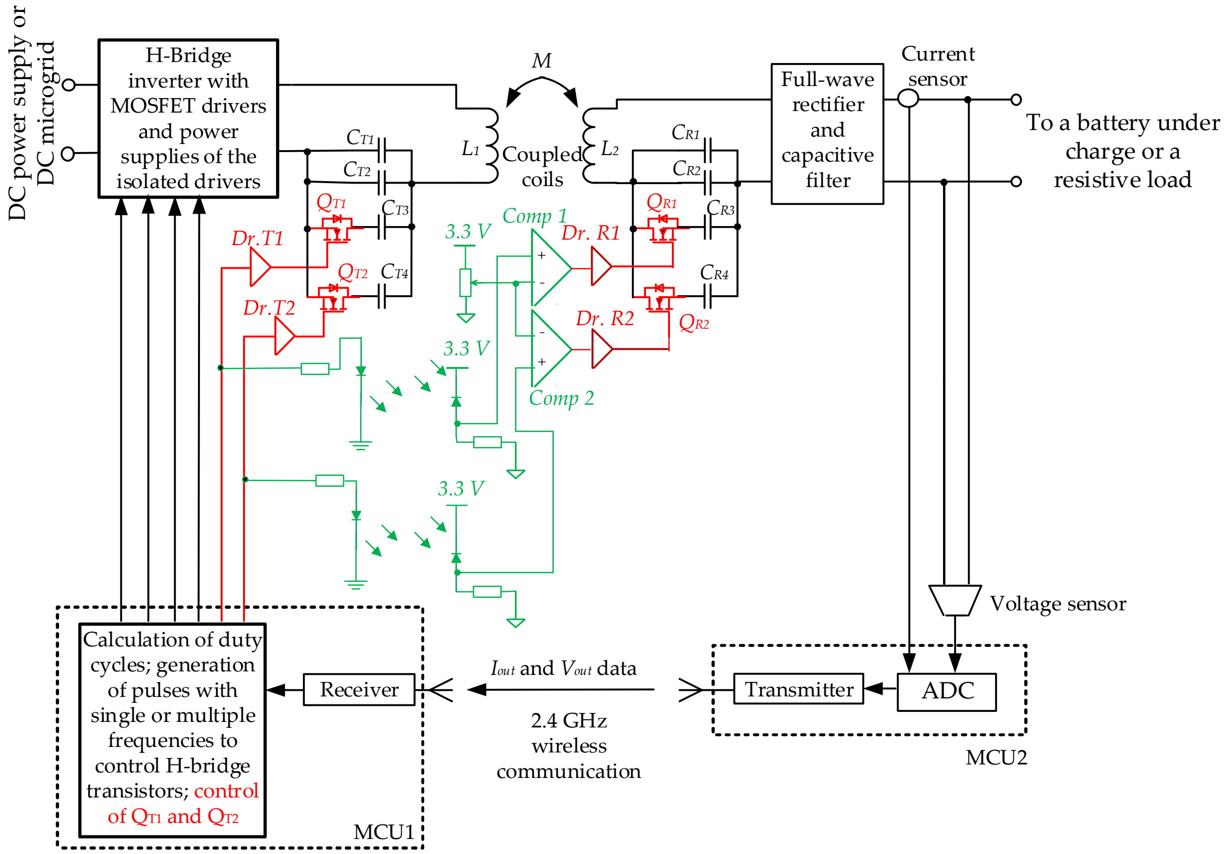

Figure 7. A block diagram of the wireless charger with the proposed approach for the performance improvements (the main modifications to the conventional wireless charger are shown in color).

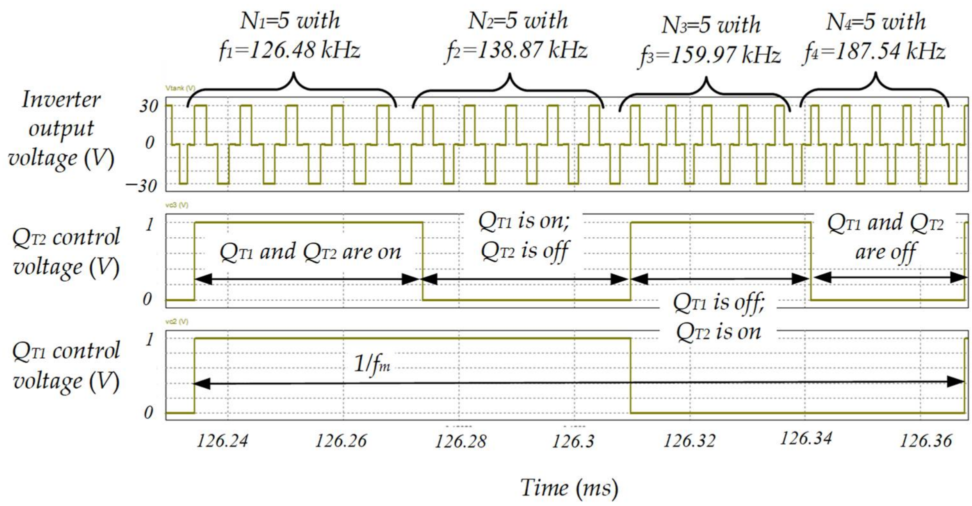

Figure 8. Simulated waveforms of the inverter output voltage and control voltages of the transistors of the resonant circuits. (In this example, the number of pulses N_x at each frequency is equal to 5 and $f_m \approx 8$ kHz).

The obtained simulation results (Figure 9 and Table 2) allow us to conclude that the wireless battery charger operating at multiple frequencies with the proposed approach for the performance improvement based on the modified control technique and modified resonant circuits has much lower peak values of the currents of the transmitting and the receiving WPT coils, a much higher (by up to 3.7 dB higher) EMI reduction coefficient (at all R_{load}), noticeably better efficiency at lower load resistances (only in CC mode and in the beginning of CV mode), and moderately lower RMS values of the currents of the transistors of the H-bridge inverter and the WPT coils (mainly in CC mode and in the beginning of CV mode) than those of the conventional wireless charger operating at multiple switching frequencies. However, the improvements come at the cost of a moderately increased number of components and noticeably lower efficiency at higher load resistances (in CV mode when $R_{load} > 25\ \Omega$). It should be noted that the components used in the circuit to implement the infrared communications (shown in green in Figure 7) should not be taken into account when calculating the increase in the number of components because they can be used in conventional wireless chargers too to activate the secondary side of the charger when AMR or AGV is within the operational range of the charger.

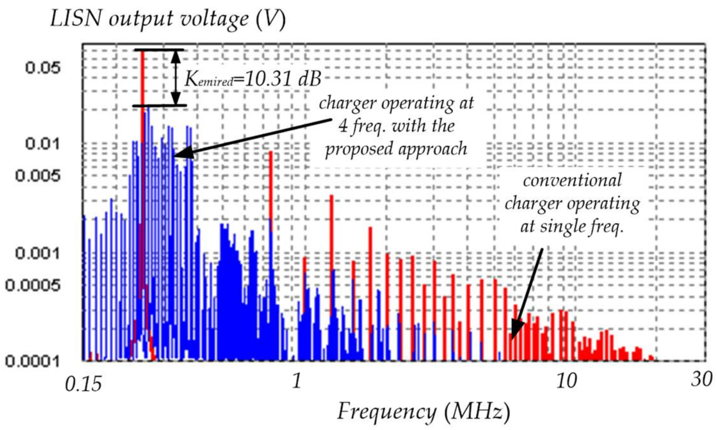

Figure 9. Simulated conducted EMI (LISN output voltage) of the conventional wireless charger operating at a single switching frequency and the wireless charger operating at multiple switching frequencies with the proposed approach for the performance improvement. (V_{in} = 25 V; $N_1 = N_2 = 3$; $N_3 = 5$; $N_4 = 9$; $f_m \approx 8$ kHz).

3. Experiments

3.1. Experimental Prototype

For the experimental studies, a scaled-down low-power prototype for the charging of 6-cell Li-ion batteries of AMR or AGV was designed according to the specifications presented in Table 1. The prototype block diagram is demonstrated in Figure 7. It can be used for comparative experimental studies of the performance of three different types of the wireless chargers: (1) the conventional wireless charger operating at a single frequency (all the transistors of the resonant circuits are on); (2) the conventional wireless charger operating at multiple frequencies (Q_{T1} and Q_{R1} are on, but Q_{T2} and Q_{R2} are off); and (3) the wireless charger with the proposed approach for the performance improvement (the transistors of the resonant circuits operate in a normal mode to tune the resonant circuits to a given switching frequency f_1, f_2, f_3, or f_4). The wireless charger is designed with the assumption that the transmitting coil will be buried in the floor, but the receiving coil is placed at the bottom of the AMR or AGV (as shown in Figure 1a). Therefore, the distance between the WPT coils will be almost fixed (2.7 cm), but there will be a lateral misalignment of the receiving coil. Since for different types of modern AMR and AGV, a positioning error usually does not exceed ±1 cm [2], it is assumed that the maximum lateral misalignment of the receiving coil is 1 cm (as shown in Figure 4).

The printed circuits boards of the primary and the secondary sides (Figure 10) of the wireless charger used in the experiments are new modified versions of those used in our previous studies [9]. The new versions of the printed circuit boards have additional components (e.g., Q_{T1}, Q_{T2}, Q_{R1}, Q_{R2}, and their drivers, the components to implement the infrared communications, etc.) and modified MCU1 code to generate two additional signals to control the transistors in the resonant circuits. The WPT coils L1 and L2 are the same as those used in [9]. The Bluetooth energy communication is used to send data from the output sensors of the wireless charger to MCU1 to implement CC or CV modes. The components of the power stage of the charger were selected by using simulations of the model of the charger in PSIM.

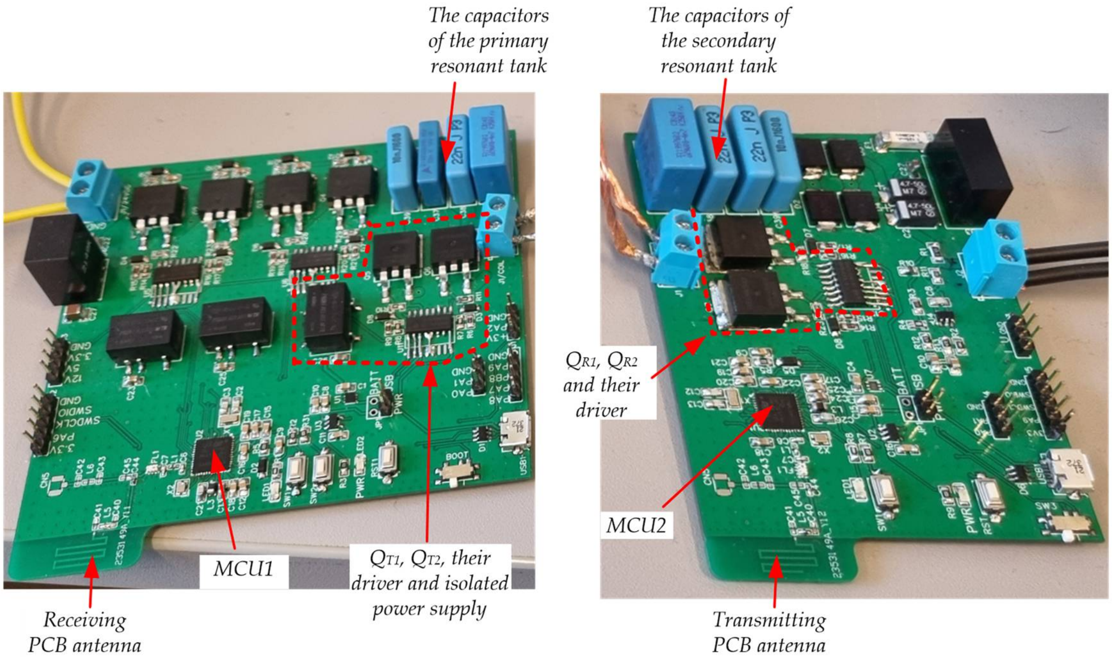

(**a**) (**b**)

Figure 10. Photos of the printed circuit boards of the designed wireless charger: (**a**) the transmitting side; (**b**) the receiving side.

Since it is assumed that the charger will be used for a 6-cell Li-ion battery charging with a discharge cut-off voltage of 22.2 V, charge cut-off voltage of 25.2 V and charging current of 2 A, the input equivalent resistance of the battery under charge will change within the range 11.1–126 Ω. During the experiments, an electronic load LD300 in constant resistance mode was used to imitate a battery under charge. The range of the load resistances 11.1–12.6 Ω corresponds to CC mode, but the range of the resistances 12.6–126 Ω corresponds to CV mode. The boundary resistance between the modes is 12.6 Ω.

The main measurements were taken for two different cases: when the WPT coils are perfectly aligned and when the coils are at the maximum misalignment. To fix the coils in the perfectly aligned position or in the maximum misaligned position, we printed two 3D plastic structures (see Figure 11).

(**a**) (**b**)

Figure 11. Photos of the plastic structures with the WPT coils: (**a**) maximum misalignment; (**b**) perfectly aligned.

In order to implement the infrared communications, two low-delay infrared-light-emitting diodes were attached to the side of the ferrite pad of the transmitting coil and four low-delay infrared photodiodes were attached to the side of the ferrite pad of the receiving coil, as is demonstrated in Figure 12. Due to the smart placement of the infrared diodes and photodiodes, the control signals of the transistors (Q_{R1} and Q_{R2}) of the secondary resonant circuit can be reliably transmitted with a small delay from the primary side of the wireless charger even if the WPT coils are misaligned. It should be noted that the infrared communication can be used to activate the secondary side of the charger when the AMR or AGV is within the operational range of the charger.

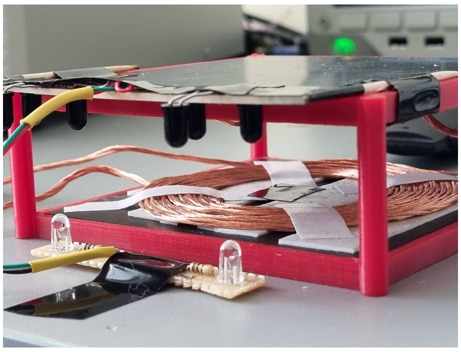

Figure 12. A photo of the WPT coils with the correctly placed infrared photodiodes and emitting diodes.

A photo of the experimental prototype with the measurement equipment connected is shown in Figure 13. In the conducted and radiated EMI measurements, a mixed-domain oscilloscope Tektronix MDO4034B with a built-in spectrum analyzer (with a peak detector) was used. To minimize the random error, an average of 16 consecutive measurement results was used. A home-made LISN circuit (described in [9]), which corresponds to a simplified version of a factory-made LISN with CISPR specifications, was also used in taking the conducted EMI measurements. A near-field H probe (Rohde & Schwarz, HZ-14, 9 kHz–30 MHz) was used to measure the radiated EMI. It was placed at a distance of 1 cm from the WPT coils. During the efficiency and the current measurements, the LISN was disconnected from the charger input. The conducted EMI was analyzed in the frequency domain according to the requirements of the international standard CISPR11: measurement frequency range 0.15 MHz–30 MHz and resolution bandwidth (RBW) 9 kHz. The radiated EMI was analyzed within the frequency range 9 kHz–30 MHz (RBW = 9 kHz).

3.2. Experimental Results and Discussion

The designed and physically built prototype of the wireless charger performs well because it can maintain CC and CV charging modes within the whole range of the input equivalent resistances of a 6-cell Li-ion battery, as may be seen in Figure 14. Similar charging profiles were obtained for all three types of the wireless chargers (the conventional chargers and the charger with the proposed approach). To better understand the proposed control technique of the modified resonant tanks, some important waveforms are depicted in Figure 15. The modulation frequency of ≈8 kHz was chosen for both types of the chargers operating at four frequencies because, as discussed in [17], for RBW = 9 kHz, the best EMI suppression can be achieved if f_m is within the range 7–9 kHz. Therefore, the total number of pulses within a modulation period is 20. The proposed wireless charger operated at $f_1 \approx 126$ kHz with $N_1 = 3$ pulses, at $f_2 \approx 138$ kHz with $N_2 = 3$ pulses, at $f_3 \approx 159$ kHz with $N_3 = 5$ pulses, and at $f_4 \approx 188$ kHz with $N_4 = 9$ pulses. Such a combination of the number of pulses gave the best EMI reduction in CC mode.

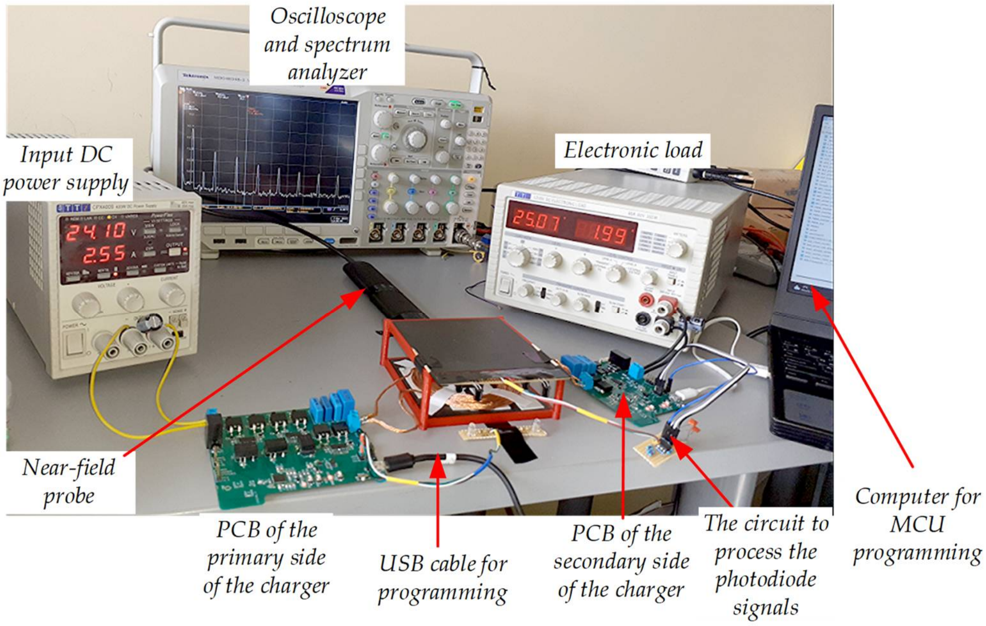

Figure 13. An image of the experimental prototype with the measurement equipment. Note: LISN is not shown.

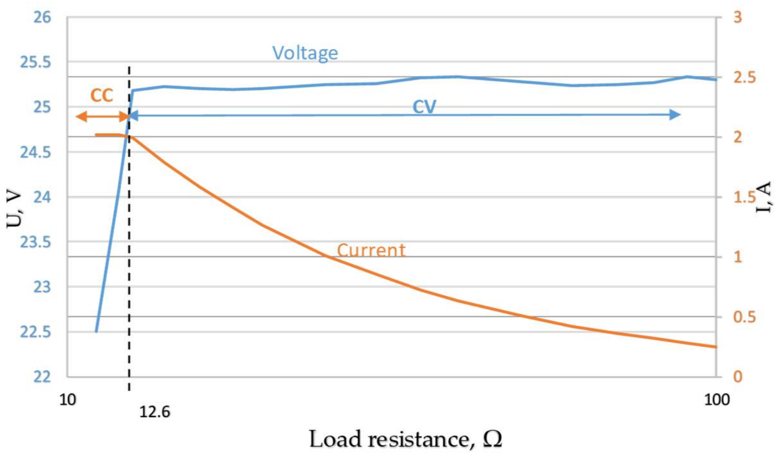

Figure 14. Charging profiles of the wireless charger.

The main experimental results are demonstrated in Tables 3 and 4 and Figures 16–19.

Table 3. The experimental results (the coils are perfectly aligned).

Parameter	R_{load} (Ω)	Classical Approach (the Charger Operates at a Single Frequency)	Classical Approach (the Charger Operates at four Frequencies w/o Modification of the Res. Tank)	Proposed Approach (the Charger Operates at four Frequencies with Modification of the Res. Tank)
K_{emired} (dB)	12.6	-	10.1	14.2
	15	-	9.3	12.06
	30	-	8.48	12.02
	40	-	8.07	10.68
	50	-	7.92	8.99
I_{peakL1} (A)	12.6	4.57	6.15	4.74
	15	4.44	6.12	4.62
	30	4.38	4.97	4.6
	40	4.36	4.88	4.58
	50	4.3	4.56	4.49

Table 3. *Cont.*

Parameter	R_{load} (Ω)	Classical Approach (the Charger Operates at a Single Frequency)	Classical Approach (the Charger Operates at four Frequencies w/o Modification of the Res. Tank)	Proposed Approach (the Charger Operates at four Frequencies with Modification of the Res. Tank)
I_{RMSL1} (A)	12.6	3.28	3.19	2.69
	15	3.24	3.06	2.68
	30	3.21	2.7	2.65
	40	3.19	2.66	2.65
	50	3.17	2.6	2.55

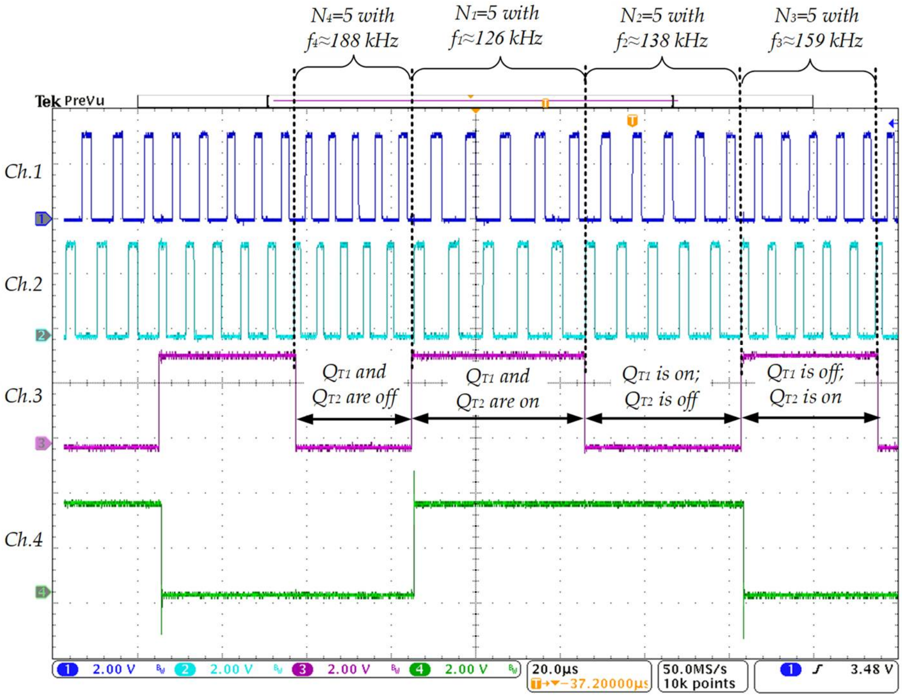

Figure 15. Experimental waveforms of the wireless charger with the proposed approach for performance improvement. Ch.1: the control voltage of the left high-side MOSFET of the H-bridge inverter; Ch.2: the control voltage of the right high-side MOSFET of the H-bridge inverter; Ch.3: the control voltage of the resonant circuit transistor Q_{T2}; Ch.4: the control voltage of the resonant circuit transistor $Q_{T1.}$ Scale: 2 V/div.; 20 µs/div.

Table 4. The experimental results (at the maximum lateral misalignment of the coils).

Parameter	R_{load} (Ω)	Classical Approach (the Charger Operates at a Single Frequency)	Classical Approach (the Charger Operates at four Frequencies w/o Modification of the Res. Tank)	Proposed Approach (the Charger Operates at four Frequencies with Modification of the Res. Tank)
K_{emired} (dB) *	12.6	-	9.01	12.46
	20	-	8.89	11.73
	30	-	8.22	10.85
	40	-	7.93	10.12
	50	-	7.31	9.57
A_{emired} (dB) **	12.6	-	3.83	5.71
	20	-	3	6.03
	30	-	2.75	6.62
	40	-	2.98	6.87
	50	-	3.27	6.84

Table 4. *Cont.*

Parameter	R_{load} (Ω)	Classical Approach (the Charger Operates at a Single Frequency)	Classical Approach (the Charger Operates at four Frequencies w/o Modification of the Res. Tank)	Proposed Approach (the Charger Operates at four Frequencies with Modification of the Res. Tank)
I_{peakL1} (A)	12.6	5.24	6.95	5.24
	20	5.12	6.12	5.17
	30	5.08	5.54	5.15
	40	5.06	5.51	5.17
	50	5.03	5.37	5.12
I_{RMSL1} (A)	12.6	3.58	3.44	2.91
	20	3.48	3.04	2.85
	30	3.45	2.91	2.87
	40	3.44	2.85	2.86
	50	3.42	2.79	2.86

* K_{emired} is the conducted EMI reduction coefficient; ** A_{emired} is the radiated EMI reduction coefficient.

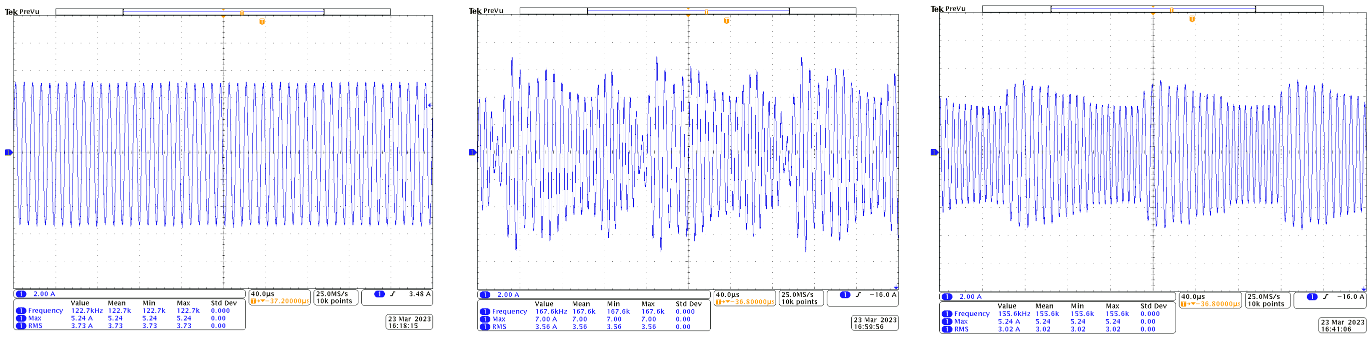

(**a**) (**b**) (**c**)

Figure 16. The experimental current waveforms of the transmitting coil for three different cases (at the worst coupling): (**a**) the conventional wireless charger operating at a single frequency; (**b**) the conventional wireless charger operating at four frequencies; and (**c**) the wireless charger operating at four frequencies with the proposed modified control technique and modified resonant tanks. Parameters: CC mode; R_{load} = 12.6 Ω; V_{in} = 25 V; $f_m \approx$ 8 kHz. Scale: 2 A/div; 40 µs/div.

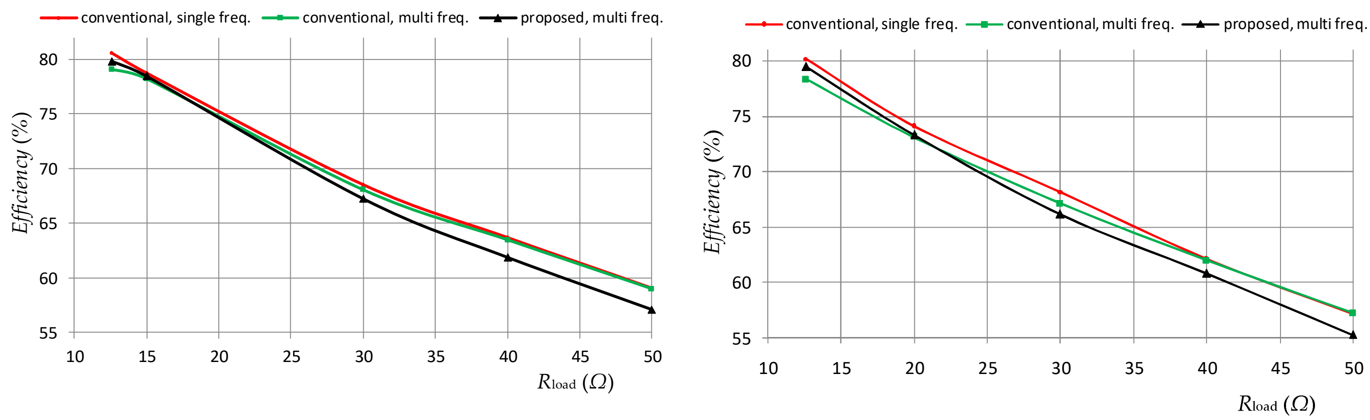

(**a**) (**b**)

Figure 17. The experimental efficiency versus the load resistance for the three different cases: the conventional wireless charger operating at a single frequency (red); the conventional wireless charger operating at four frequencies (green); the wireless charger operating at four frequencies with the proposed modified resonant tank (black). (**a**) The coils are aligned perfectly; (**b**) the misalignment of the coils is at its maximum. Parameters: V_{in} = 25 V.

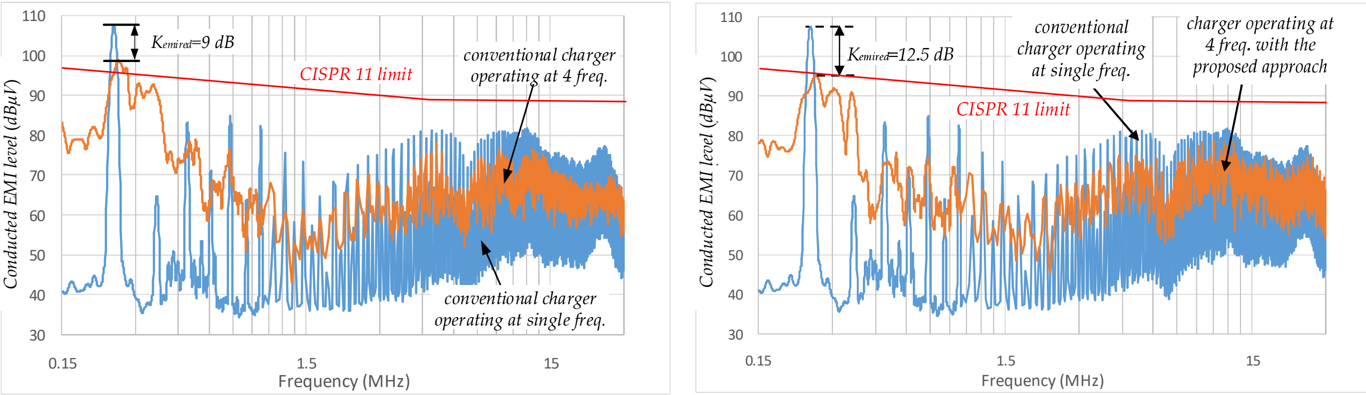

(**a**) (**b**)

Figure 18. Experimental conducted EMI of (**a**) the conventional wireless charger operating at a single or four switching frequencies and (**b**) the conventional wireless charger operating at a single switching frequency and the wireless charger operating at multiple switching frequencies with the proposed approach for the performance improvement. (The maximum misalignment of the coils; V_{in} = 25 V; R_{load} = 12.6 Ω; modulation frequency $f_{\mathrm{m}} \approx 8$ kHz).

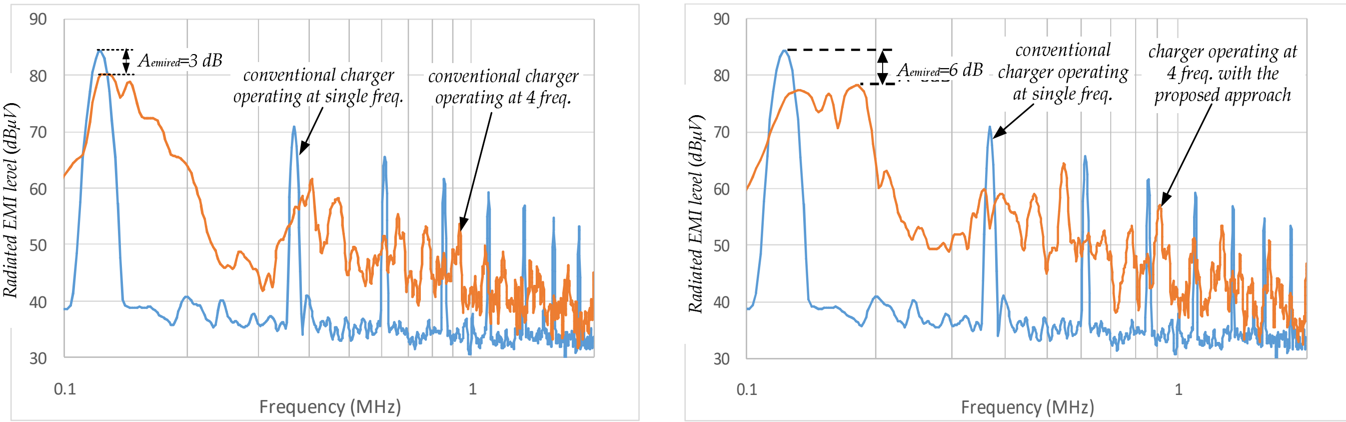

(**a**) (**b**)

Figure 19. Experimental radiated EMI (0.1–2 MHz) of (**a**) the conventional wireless charger operating at a single or four switching frequencies and (**b**) the conventional wireless charger operating at a single switching frequency and the wireless charger operating at multiple switching frequencies with the proposed approach for the performance improvement. (The worst-case coupling; V_{in} = 25 V; R_{load} = 20 Ω; modulation frequency $f_{\mathrm{m}} \approx 8$ kHz). Note: the radiated EMI here represents the output voltage (expressed in dBµV) of the near-field probe without considering the antenna factor of the probe. If it is necessary to show the radiated EMI expressed in dBµA/m and to compensate for the probe frequency characteristics, one should take into account the antenna factor of the probe as described, e.g., in [5].

From the results, we can conclude that:

- The experimental results confirm the simulation results that the proposed approach for the improvement of the performance of the wireless charger gives much better (up to 4.1 dB higher) conducted EMI reduction coefficient at every R_{load} (see Tables 3 and 4 and Figure 18). Moreover, the proposed wireless charger's conducted EMI levels are in compliance with CISPR11 Group 1 Class A Q-peak standard limits (see Figure 18) within the whole range of R_{load} (EMI filter can be eliminated), but the conducted EMI of the conventional wireless charger operating at either a single or four frequencies does not comply with CISPR11 Group 1 Class A standard requirements, especially in CC mode (EMI filter still should be used). The experimental results, similar to the simulation results, also show that the difference between the conducted EMI reduction coefficients decreases as the R_{load} increases. However, the simulation model cannot accurately predict K_{emired}, mainly because we did not know the actual values of the parasitic resistances of the capacitors (especially the input capacitor) and the coils.

- The proposed approach for the improvement of the performance of the wireless charger also gives a much better (up to 3.5 dB higher) reduction coefficient of the fundamental (the most dominant) harmonic of the radiated EMI at every R_{load} (see Table 4 and Figure 19).
- The wireless charger with the proposed approach for the performance improvement also has much lower peak values of the currents of the WPT coils at a lower R_{load} (in CC mode and in the beginning of CV mode) than those of the conventional wireless charger operating at multiple frequencies. However, the proposed approach gives only a moderate reduction in the peak values at higher load resistances ($R_{\text{load}} > 40\ \Omega$). A comparison of the simulated and experimental peak values revealed that there is moderate agreement between the results (difference <10%). The peak values can be predicted with moderate accuracy.
- The wireless charger with the proposed approach for the performance improvement also has noticeably lower RMS values of the currents of the WPT coils at a lower R_{load} (in CC mode and in the beginning of CV mode) than those of the conventional wireless charger operating either at multiple frequencies or a single frequency. However, the RMS values of the currents of the proposed wireless charger are very similar to those of the conventional wireless charger operating at multiple frequencies at higher load resistances ($R_{\text{load}} > 40\ \Omega$). The experimental RMS values are in good agreement with the simulated results. The simulation model can be used for accurate prediction of RMS values of the currents of the power components.
- The experimental results (Figure 17) also confirm the simulation results that the wireless charger with the proposed approach for the performance improvement has noticeably higher efficiency (by up to 1.4%) at a lower R_{load} (in CC mode and in the beginning of CV mode, especially at the maximum misalignment) than that of the conventional wireless charger operating at multiple frequencies. However, in contrast to the simulation results, the experimental results show that the wireless charger with the proposed approach for the performance improvement has noticeably lower efficiency at a higher R_{load} (CV mode, $R_{\text{load}} > 30\ \Omega$) than that of the conventional wireless chargers operating at either a single or multiple switching frequencies. Moreover, the experimental results also show that the efficiency of the conventional wireless charger operating at multiple frequencies (with Q_{T1} and Q_{R1} "on", but Q_{T2} and Q_{R2} "off") is not noticeably higher than that of the conventional wireless charger operating at a single frequency, but the efficiencies are very similar at higher load resistances ($R_{\text{load}} > 35\ \Omega$). The experiments also revealed that when Q_{T1}, Q_{R1}, Q_{T2}, and Q_{R2} are "on", the efficiency of the conventional wireless charger operating at multiple frequencies is noticeably higher than that of the conventional wireless charger operating at a single frequency. The simulation model cannot accurately predict the efficiency because we did not know actual values of the parasitic resistances of the power components and we did not take into account the switching losses and losses in the ferrite pads.

Based on the analysis presented, if the efficiency at higher load resistances is of importance, our recommendation is to change the resonant circuits from the proposed configuration to the conventional configuration when $R_{\text{load}} > 30\ \Omega$ (in our case). This can be achieved by keeping all transistors of the resonant circuits in the "on" state constantly or by keeping only Q_{T1} and Q_{R1} "on" constantly.

4. Conclusions

The simulation and the experimental results clearly demonstrated that the wireless battery charger operating at multiple switching frequencies with the proposed approach for the performance improvement has numerous advantages over the conventional wireless charger operating at multiple switching frequencies. It has much lower peak values of the currents of the transmitting and the receiving WPT coils, especially at lower load resistances (in CC or in the beginning of CV modes), it has higher conducted and radiated EMI reduction coefficients (at every R_{load}), it has noticeably better efficiency at lower load resistances (only in CC mode and in the beginning of CV mode), and moderately lower RMS values of the currents of the transistors of the H-bridge inverter and the WPT coils (mainly in CC mode and in the beginning of CV mode). The proposed approach for the performance improvement is based on the modified resonant tanks that are tuned to a given switching frequency. However, the improvements come at the cost of a moderately increased number of components and noticeably lower efficiency at higher load resistances (in CV mode when $R_{load} > 25\ \Omega$). If high efficiency is of concern at higher load resistances, our recommendation is to change the resonant circuits from the proposed configuration to the conventional configuration automatically when $R_{load} > 30\ \Omega$. This can be achieved by keeping all transistors of the resonant circuits in the "on" state constantly or by keeping only Q_{T1} and Q_{R1} "on" constantly.

Author Contributions: Conceptualization, D.S.; methodology, D.S. and O.C.; software and design, A.S.; validation, A.S. and D.S.; formal analysis, D.S. and O.C.; data curation, A.S.; writing—original draft preparation, D.S.; writing—review and editing, J.Z.; visualization, D.S.; supervision, J.Z.; project administration, J.Z. All authors have read and agreed to the published version of the manuscript.

Funding: This work was supported by the European Regional Development Fund within the Activity 1.1.1.2 "Post-doctoral Research Aid" of the Specific Aid Objective 1.1.1 "To increase the research and innovative capacity of scientific institutions of Latvia and the ability to attract external financing, investing in human resources and infrastructure" of the Operational Programme "Growth and Employment" (No.1.1.1.2/VIAA/3/19/415).

Data Availability Statement: Data of our study are available upon request.

Conflicts of Interest: The authors declare no conflict of interest. The funders had no role in the design of the study, in the collection, analyses, or interpretation of data, in the writing of the manuscript, or in the decision to publish the results.

References

1. Li, Y.; Duan, Q.; Zou, Y. High Robustness Control for Robotic Wireless Power Transfer Systems with Multiple Uncertain Parameters Using a Virtual Buck Converter. *Energies* **2017**, *10*, 517. [CrossRef]
2. AGV Navigation: Methods, Comparison, Pros and Cons—Illustrated Guide. Available online: https://www.agvnetwork.com/types-of-navigation-systems-automated-guided-vehicles (accessed on 10 April 2023).
3. Mohammadpour, M.; Zeghmi, L.; Kelouwani, S.; Gaudreau, M.-A.; Amamou, A.; Graba, M. An Investigation into the Energy-Efficient Motion of Autonomous Wheeled Mobile Robots. *Energies* **2021**, *14*, 3517. [CrossRef]
4. Oitzman, M. A Guide to the Latest in Mobile Robot Technology at IMTS 2018. Robotics Business Review. 11 September 2018. Available online: https://www.controleng.com/articles/mobile-platform-can-be-used-as-base-for-mobile-machining/ (accessed on 9 April 2023).
5. Stepins, D.; Zakis, J.; Padmanaban, P.; Deveshkumar Shah, D. Suppression of Radiated Emissions from Inductive-Resonant Wireless Power Transfer Systems by Using Spread-Spectrum Technique. *Electronics* **2022**, *11*, 730. [CrossRef]
6. Zimmer, S.; Helwig, M.; Winkler, A.; Modler, N. Modeling Electrical Conductivity of Metal Meshes for Predicting Shielding Effectiveness in Magnetic Fields of Wireless Power Transfer Systems. *Electronics* **2022**, *11*, 2156. [CrossRef]
7. Suzuki, M. Conducted Emission in an 85 kHz, 50 kW WPT System with Opposite-Phase Transfer and Spread Spectrum. In Proceedings of the 2019 IEEE PELS Workshop on Emerging Technologies: Wireless Power Transfer (WoW), London, UK, 18–21 June 2019; pp. 1–4.
8. Inoue, K.; Kusaka, K.; Itoh, J. Reduction in Radiation Noise Level for Inductive Power Transfer Systems using Spread Spectrum Techniques. *IEEE Trans. Power Electr.* **2018**, *33*, 3076–3085. [CrossRef]
9. Stepins, D.; Sokolovs, A.; Zakis, J. Thorough Study of Multi-Switching-Frequency-Based Spread-Spectrum Technique for Suppression of Conducted Emissions from Wireless Battery Chargers. *Electronics* **2023**, *12*, 687. [CrossRef]
10. Simonazzi, M.; Sandrolini, L. Conducted Emission Analysis of a Near-Field Wireless Power Transfer System. In Proceedings of the IEEE 15th International Conference on Compatibility, Power Electronics and Power Engineering (CPE-POWERENG), Florence, Italy, 14–16 July 2021; pp. 1–6.

11. Lin, J.-Y.; Hsu, Y.-C.; Lin, Y.-D. A Low EMI DC-DC Buck Converter with a Triangular Spread-Spectrum Mechanism. *Energies* **2020**, *13*, 856. [CrossRef]
12. Pareschi, F.; Rovatti, R.; Setti, G. EMI reduction via spread spectrum in DC/DC converters: State of the art, optimization, and tradeoffs. *IEEE Access* **2015**, *3*, 2857–2874. [CrossRef]
13. Ouseph, C.; Stepins, D.; Zakis, J. Frequency-Modulated Inductive-Resonant WPT System with Improved Efficiency. In Proceedings of the 19th IEEE International Power Electronics and Motion Control Conference (PEMC2020), Gliwice, Poland, 25–29 April 2021; pp. 1–8.
14. Shevchenko, V.; Pakhaliuk, B.; Zakis, J.; Veligorskyi, O.; Luszcz, J.; Husev, O.; Lytvyn, O.; Matiushkin, O. Closed-Loop Control System Design for Wireless Charging of Low-Voltage EV Batteries with Time-Delay Constraints. *Energies* **2021**, *14*, 3934. [CrossRef]
15. Cho, K.; Park, W.; Hong, M.; Park, G.; Cho, W.; Seo, J.; Han, K. Analysis of Latency Performance of Bluetooth Low Energy (BLE) Networks. *Sensors* **2015**, *15*, 59–78. [CrossRef]
16. Gati, E.; Kampitsis, G.; Manias, S. Variable Frequency Controller for Inductive Power Transfer in Dynamic Conditions. *IEEE Trans. Power Electron.* **2017**, *32*, 1684–1696. [CrossRef]
17. Stepins, D. An improved control technique of switching frequency modulated power factor correctors for low THD and high power factor. *IEEE Trans. Power Electr.* **2016**, *31*, 5201. [CrossRef]